Journal of Molecular Graphics and Modelling 54 (2014) 174–183

Contents lists available at ScienceDirect

Journal of Molecular Graphics and Modelling

journal homepage: www.elsevier.com/locate/JMGM

# Multi-generational pharmacophore modeling for ligands to the cholane steroid-recognition site in the $\beta_1$ modulatory subunit of the $BK_{Ca}$ channel

Jacob E. McMillan[a], Anna N. Bukiya[b], Camisha L. Terrell[c], Shivaputra A. Patil[c], Duane D. Miller[c], Alex M. Dopico[b], Abby L. Parrill[a,*]

[a] Department of Chemistry and Computational Research on Materials Institute (CROMIUM), The University of Memphis, Memphis, TN 38152, USA
[b] Department of Pharmacology, College of Medicine, The University of Tennessee Health Sciences Center, Memphis, TN 38163, USA
[c] Department of Pharmaceutical Sciences, College of Pharmacy, The University of Tennessee Health Sciences Center, Memphis, TN 38163, USA

ARTICLE INFO

*Article history:*
Accepted 15 October 2014
Available online 24 October 2014

*Keywords:*
BKCa channel
Beta subunit
Pharmacophore model

ABSTRACT

Large conductance, voltage- and $Ca^{2+}$-gated $K^+$ ($BK_{Ca}$) channels play a critical role in smooth muscle contractility and thus represent an emerging therapeutic target for drug development to treat vascular disease, gastrointestinal, bladder and uterine disorders. Several compounds are known to target the ubiquitously expressed $BK_{Ca}$ channel-forming α subunit. In contrast, just a few are known to target the $BK_{Ca}$ modulatory $\beta_1$ subunit, which is highly expressed in smooth muscle and scarce in most other tissues. Lack of available high-resolution structural data makes structure-based pharmacophore modeling of $\beta_1$ subunit-dependent $BK_{Ca}$ channel activators a major challenge. Following recent discoveries of novel $BK_{Ca}$ channel activators that act via $\beta_1$ subunit recognition, we performed ligand-based pharmacophore modeling that led to the successful creation and fine-tuning of a pharmacophore over several generations. Initial models were developed using physiologically active cholane steroids (bile acids) as template. However, as more compounds that act on $BK_{Ca}$ $\beta_1$ have been discovered, our model has been refined to improve accuracy. Database searching with our best-performing model has uncovered several novel compounds as candidate $BK_{Ca}$ $\beta_1$ subunit ligands. Eight of the identified compounds were experimentally screened and two proved to be activators of recombinant $BK_{Ca}$ $\beta_1$ complexes. One of these activators, sobetirome, differs substantially in structure from any previously reported activator.



## 1. Introduction

Functional $BK_{Ca}$ channels result from homomeric assembly of four α (slo, slo1) subunits. In most tissues, however, the native channel complex includes modulatory β subunits that modify ion channel phenotype [1]. Due to the ubiquitous expression of the $BK_{Ca}$ channel-forming α subunit, these channels play a significant role in many physiological functions including neuronal excitability, neurotransmission, hormonal secretion and regulation of smooth muscle tone [2,3]. $BK_{Ca}$ α subunits consist of seven transmembrane segments [4] in addition to a long C-terminal tail that recognizes several physiologic ligands, including intracellular $Ca^{2+}$ [5]. In contrast, $BK_{Ca}$ β types ($\beta_{1-4}$) are small proteins, each made of intracellular N- and C-termini, and two transmembrane helices connected by a large extracellular loop [6].

Differential expression of β subunit types across tissues allows tissue-specific $BK_{Ca}$ current phenotypes that contribute to cell physiology in a rather tissue-specific manner. In particular, when co-expressed with the α subunit, the smooth muscle-abundant $\beta_1$ subunit increases the channel's apparent $Ca^{2+}$ sensitivity and slows down channel gating kinetics [7]. In smooth muscle, an increase in the channel's apparent $Ca^{2+}$ sensitivity allows $BK_{Ca}$ channels to activate upon increase in intracellular $Ca^{2+}$ levels near the $BK_{Ca}$ channel, which are raised during membrane depolarization and smooth muscle contraction. Thus, $BK_{Ca}$ channel activation results in outward $K^+$ currents that tend to hyperpolarize the membrane and oppose depolarization-induced $Ca^{2+}$ entry. Eventually, smooth muscle contraction is restrained and relaxation is facilitated [6,7]. Moreover, the critical role of $BK_{Ca}$ $\beta_1$ subunit in smooth muscle physiology has been well

* Corresponding author. Tel.: +1 9016783371; fax: +1 901 678 4831.
*E-mail addresses:* jemcmlln@memphis.edu (J.E. McMillan), abukiya@uthsc.edu (A.N. Bukiya), cterrell@cbu.edu (C.L. Terrell), spatil3@uthsc.edu (S.A. Patil), dmiller@uthsc.edu (D.D. Miller), adopico@uthsc.edu (A.M. Dopico), aparrill@memphis.edu (A.L. Parrill).

http://dx.doi.org/10.1016/j.jmgm.2014.10.008
1093-3263/

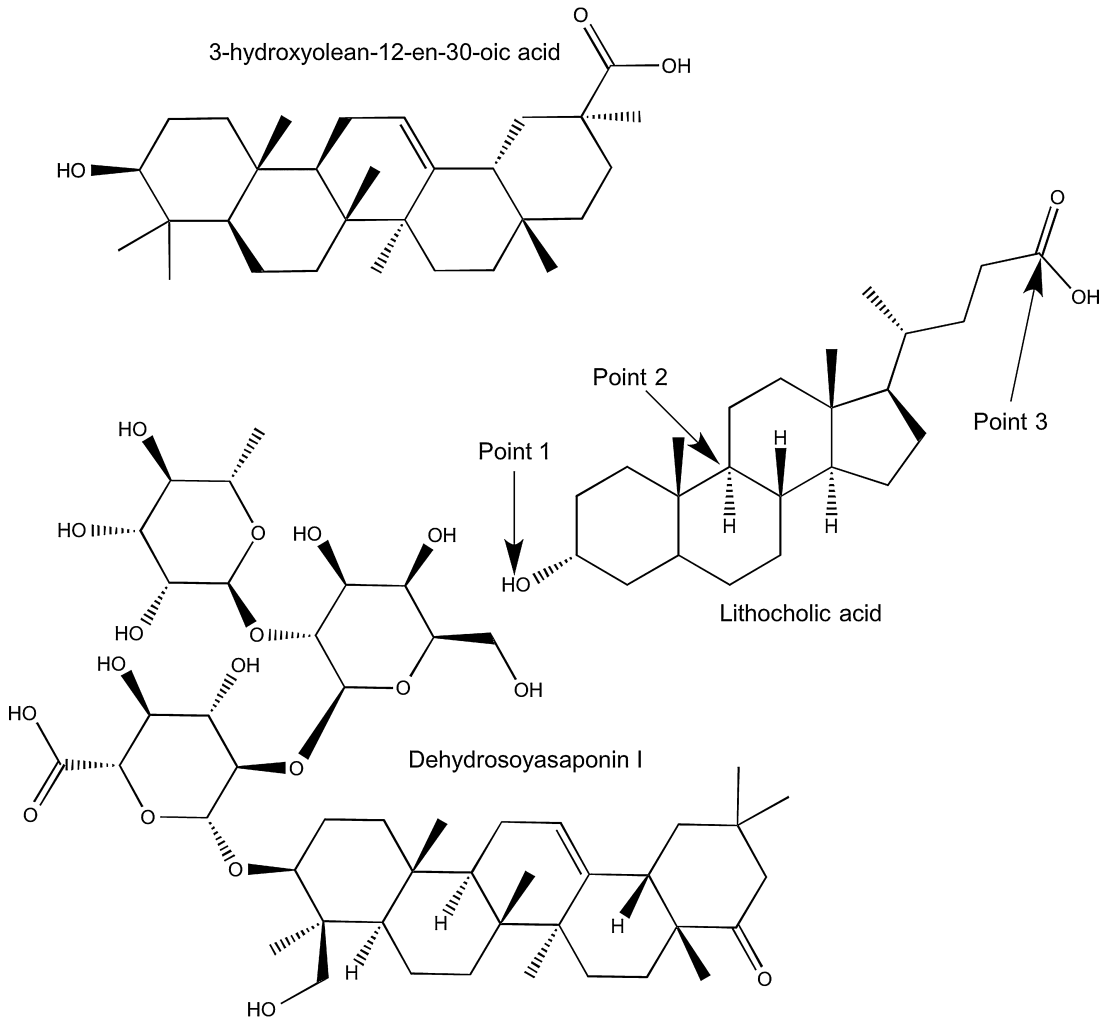


**Fig. 1.** $BK_{Ca}$ $\beta_1$ selective activators; lithocholic acid (LCA), 3-hydroxyolean-12-en-30-oic acid (3-HENA), and dehydrosoyasaponin I (DHS-I).

documented: for instance, $BK_{Ca}$ $\beta_1$ knock-out mice are characterized by increased arterial tone [7]. Decreased $\beta_1$ gene expression leads to systemic hypertension in rats [8] and increased phasic contractions in mouse urinary bladder [9]. Considering the key role of $BK_{Ca}$ $\beta_1$ in determining smooth muscle tone, this subunit represents an attractive target for therapeutic developments against a wide clinical spectrum of prevalent human conditions associated with enhanced smooth muscle contraction, including bronchial asthma, systemic hypertension, cerebral vasospasm, erectile dysfunction, premature labor, and some bladder disorders [10–12].

There are several compounds known to modify $BK_{Ca}$ channel function, yet only a few are confirmed to act via the recently identified $\beta_1$ subunit cholane steroid-recognition site (Fig. 1) [13,14]. Cholane steroids such as the bile acid, lithocholic acid (LCA), increase $BK_{Ca}$ channel activity through interaction with $\beta_1$ subunits [14]. This action is $\beta_1$ subunit-specific and not observed with $\beta_{2-4}$ subunit-containing $BK_{Ca}$ complexes or with homomeric $\alpha$ channels [15]. Combined results from point mutagenesis, electrophysiology and computational modeling indicate that the cholane steroid-recognition site is located in the $\beta_1$ subunit second transmembrane domain, with Thr169 playing a critical role in bile acid recognition [16]. Previous structure-activity relationship (SAR) studies indicated that the overall shape of the bile acid, as well as the number of hydroxyls, and placement of hydroxyls and carboxylic acids, were important in bile acid interaction with $\beta_1$ [14]. Among non-steroidal compounds, only one triterpenoid, 3-hydroxyolean-12-en-30-oic acid (3-HENA) [13] has been reported to specifically target $\beta_1$-containing $BK_{Ca}$ complexes. Moreover, although there are several ligands with $\beta_1$-dependent effects on $BK_{Ca}$ channel opening, only LCA and 3-HENA have been reported to interact with a defined recognition site [13] making the other ligands less useful in determination of a pharmacophore.

High-resolution structures of the $BK_{Ca}$ $\alpha$ gating-ring are available [17], however structures of neither the complete $\alpha$ subunit nor any $\beta$ subunit are available. Given this deficit in receptor structural data, the present study focuses on ligand-based pharmacophore model development using $BK_{Ca}$-ligand structures found by our group to selectively target the cholane steroid-recognition site in $BK_{Ca}$ $\beta_1$. As new data and techniques have become available, multiple iterations of pharmacophore modeling have led to a better understanding of how pharmacophore features effect model performance, yet lack of structural diversity amongst known ligands has posed a significant challenge. The best performing model was used to search the PubChem compound database [18], which led to the confirmation of two novel active compounds that fit structural criteria posed by the $\beta_1$ steroid-sensing site while offering structural diversity over known ligands. The expanded structural diversity provided by these new $BK_{Ca}$ channel activators sets the stage for future pharmacophore model refinements as well as further pharmacological characterization of these new biologically active compounds.

## 2. Methods

### 2.1. Pharmacophore model development

Initial modeling was performed using the Molecular Operating Environment (MOE)[19] 2006.08 software package. Stochastic conformational searching was performed on LCA (Fig. 2 **#14**) using the MMFF94x forcefield, chosen for its ubiquitous use with small organic molecules, with gas phase solvation and a dielectric of zero. MMFF94x is an unpublished version of the MMFF94 forcefield [20] where conjugated nitrogen atoms are treated as planar instead of tetrahedral. The carboxylic acid of LCA was

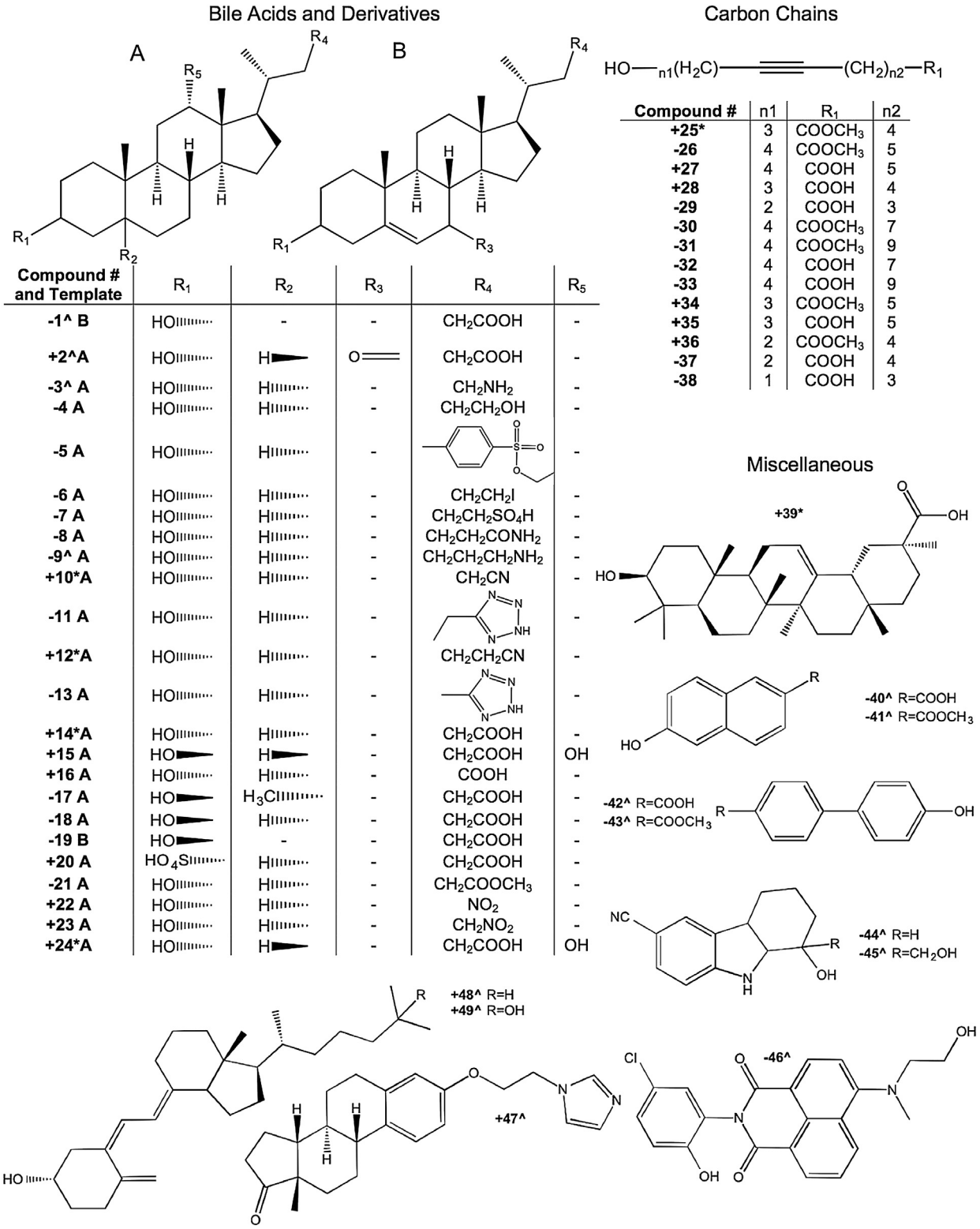


| Compound # | n1 | $R_1$ | n2 |
|---|---|---|---|
| +25* | 3 | $COOCH_3$ | 4 |
| -26 | 4 | $COOCH_3$ | 5 |
| +27 | 4 | COOH | 5 |
| +28 | 3 | COOH | 4 |
| -29 | 2 | COOH | 3 |
| -30 | 4 | $COOCH_3$ | 7 |
| -31 | 4 | $COOCH_3$ | 9 |
| -32 | 4 | COOH | 7 |
| -33 | 4 | COOH | 9 |
| +34 | 3 | $COOCH_3$ | 5 |
| +35 | 3 | COOH | 5 |
| +36 | 2 | $COOCH_3$ | 4 |
| -37 | 2 | COOH | 4 |
| -38 | 1 | COOH | 3 |

| Compound # and Template | $R_1$ | $R_2$ | $R_3$ | $R_4$ | $R_5$ |
|---|---|---|---|---|---|
| -1^ B | HO | - | - | $CH_2COOH$ | - |
| +2^A | HO | H | O | $CH_2COOH$ | - |
| -3^ A | HO | H | - | $CH_2NH_2$ | - |
| -4 A | HO | H | - | $CH_2CH_2OH$ | - |
| -5 A | HO | H | - |  | - |
| -6 A | HO | H | - | $CH_2CH_2I$ | - |
| -7 A | HO | H | - | $CH_2CH_2SO_4H$ | - |
| -8 A | HO | H | - | $CH_2CH_2CONH_2$ | - |
| -9^ A | HO | H | - | $CH_2CH_2CH_2NH_2$ | - |
| +10*A | HO | H | - | $CH_2CN$ | - |
| -11 A | HO | H | - |  | - |
| +12*A | HO | H | - | $CH_2CH_2CN$ | - |
| -13 A | HO | H | - |  | - |
| +14*A | HO | H | - | $CH_2COOH$ | - |
| +15 A | HO | H | - | $CH_2COOH$ | OH |
| +16 A | HO | H | - | COOH | - |
| -17 A | HO | $H_3C$ | - | $CH_2COOH$ | - |
| -18 A | HO | H | - | $CH_2COOH$ | - |
| -19 B | HO | - | - | $CH_2COOH$ | - |
| +20 A | $HO_4S$ | H | - | $CH_2COOH$ | - |
| -21 A | HO | H | - | $CH_2COOCH_3$ | - |
| +22 A | HO | H | - | $NO_2$ | - |
| +23 A | HO | H | - | $CH_2NO_2$ | - |
| +24*A | HO | H | - | $CH_2COOH$ | OH |

**Fig. 2.** Compounds used in pharmacophore model development and testing. Active compounds are indicated with a+ before the compound number. Inactive compounds are indicated with a− before the compound number. The most active compounds are denoted with an *. Compounds denoted with a ^ indicate previously unpublished compounds whose synthesis and/or electrophysiology are included in the supplementary material.

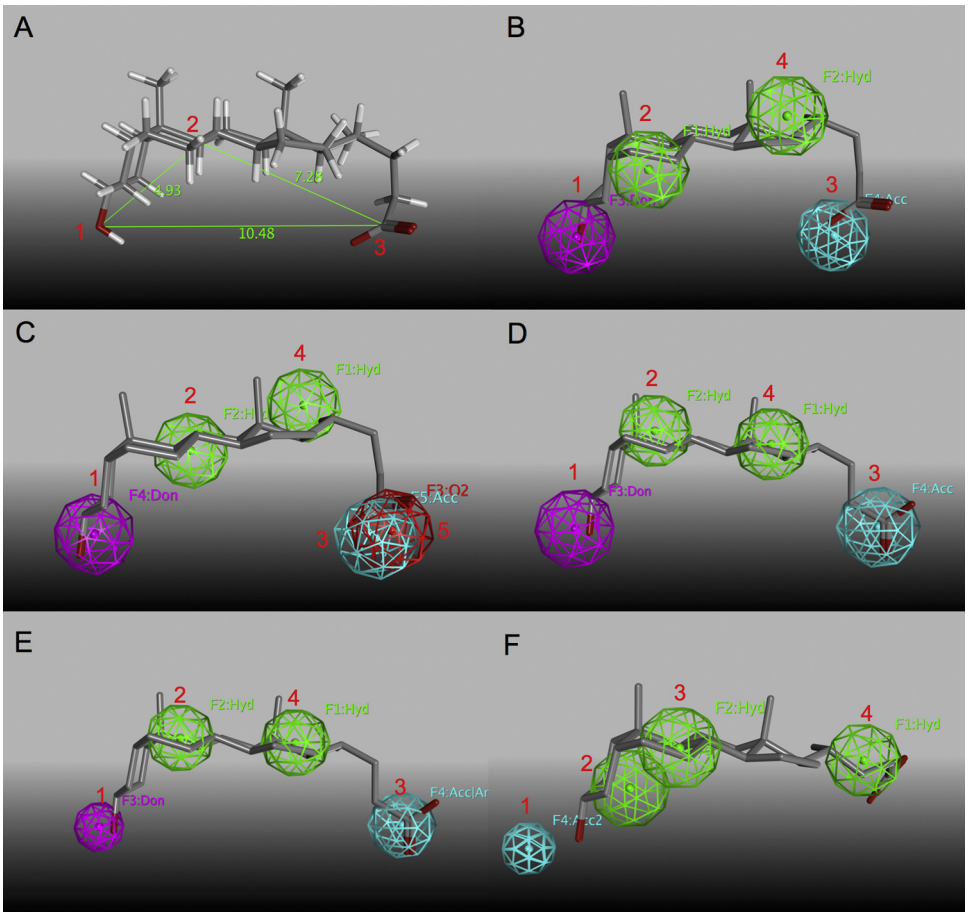


**Fig. 3.** Lithocholic acid is mapped to all generations of pharmacophore models for comparison. Magenta features represent hydrogen bond donors, green features represent hydrophobic centers, teal features represent hydrogen bond acceptors, and the red feature represents a carboxylic acid bioisostere. In the 5th generation model (panel E) the teal feature is a combination of a hydrogen bond acceptor and an anion. In the 6th generation model the teal feature is a hydrogen bond acceptor projection from overlapped hydrogen bond donors in the model training set. (A) 1st generation crude model of pharmacophore using atomic distances. (B) 2nd generation model developed for conformational database searching. (C) 3rd generation model using five pharmacophore features. (D) 4th generation model generated with more structurally diverse compounds. (E) 5th generation model with volume reduced pharmacophore features. (F) 6th generation model using ligand projections for a hydrogen bond acceptor (1) and three hydrophobic features (2–4).

deprotonated to represent the expected prevalent ionization state of the molecule at physiological pH. Since LCA was reported to be the best activator among the 13 bile acids tested in a previous SAR study [14], the lowest energy conformation of LCA was used to establish distance constraints (Fig. 3A) for crude pharmacophore searching in the National Cancer Institute (NCI) database (http://cactus.nci.nih.gov/ncidb2.2/) using the 3D search feature. Hits selected in this manner proved largely to be unavailable for screening, providing incentive to develop pharmacophore models that could be used to search alternative collections of commercially available compounds.

A 2nd generation model (Fig. 3B) was generated using the pharmacophore elucidator feature in MOE 2009.10 to allow for searching of databases other than the NCI database. LCA and deoxycholic acid (**#24**), previously established activators of $\beta_1$-containing $BK_{Ca}$ channels, were used as positive examples on which to train the model. Three additional bile acids that do not increase channel activity (**#16, 17, 18**) were used as negative examples.

After the discovery of 3-HENA (**#39**) as a non-steroidal $\beta_1$ activator, a 3rd generation model was developed due to the structural diversity offered by 3-HENA [13]. The 3rd generation model (Fig. 3C) was generated using LCA and 3-HENA as active compounds, while using two new compounds as inactive compounds to train the model (**#8**, **46**) in addition to **#17**, which was used as an inactive compound in the previous generation. These compounds were selected to provide more structural diversity over inactive compounds used to train the 2nd generation model.

The 4th generation model (Fig. 3D) was obtained using LCA (**#24**), 3-HENA (**#39**), and a synthetic bile acid containing a cyano functional group in place of the lateral chain carboxylic acid (**#10**) as active compounds. Three inactive compounds were selected for structural diversity, which are shown in Fig. 2 as compounds **#1, 42, 45**.

Refinements were made to the 4th generation model to yield a 5th generation model (Fig. 3E), as follows. (1) The radii of the pharmacophore features were reduced to be more exclusive, (2) the hydrogen bond acceptor feature was changed to include anionic compounds, (3) feature 2 was moved to align better with the steroid nucleus, and (4) features 1, 3, and 4 were made "essential" features. Thus, any screened compound would contain at least these three of the four features.

Finally, a 6th generation model was developed using newer techniques available in the MOE 2013.08 software that include ligand projection features for hydrogen bond donors and acceptors. The same training set of compounds used to develop models 4 and 5 was used to develop model 6 (Fig. 3F).

### 2.2. Model evaluation

Test set compounds were compiled from various publications [14,21–23] and previously unpublished data. Electrophysiology data and synthetic schemes for unpublished compounds are provided as supplemental material. A conformational database was generated for test set compounds using LowModeMD conformational searching [24] and the MMFF94x forcefield in MOE 2013.08. Conformations were discarded if their internal energy exceeded the lowest energy conformation by 50 kcal/mol to provide more conformational diversity over the default 7 kcal/mol cutoff. The entire set of compounds used to train any generation of pharmacophore model (compounds **#1, 8, 10, 14, 16, 17, 18, 24, 39, 42, 45, and 46**) were removed from the standard test set and 37 compounds remained to calculate pharmacophore validation metrics for a common test set to allow comparison of model performance. Sensitivity, specificity, percent yield of actives, enrichment, and accuracy were calculated for each model, as discussed in detail by Triballeau et al. [25] Sensitivity (Eq. (1)) represents the ability of the model to correctly pick out actives, while specificity (Eq. (2)) indicates the model's ability to correctly reject inactive compounds. The yield of actives (Eq. (3)) indicates the proportion of active molecules selected by the model. Enrichment (Eq. (4)) is a measure of how well the model enriches the hit list with actives compared to the proportion of actives in the whole test set. Accuracy (Eq. (5)) is a measure of how well the model can discriminate between experimentally active and inactive compounds. A brief description of the calculations is given below:

$$\text{Sensitive} = \frac{\text{TP}}{\text{TP} + \text{FN}} \tag{1}$$

$$\text{Specificity} = \frac{\text{TN}}{\text{TN} + \text{FP}} \tag{2}$$

$$\text{Yield of Actives} = \frac{\text{TP}}{n} \tag{3}$$

$$\text{Enrichment} = \frac{\text{TP}/n}{A/N} \tag{4}$$

$$\text{Accuracy} = \frac{\text{TP} + \text{TN}}{N} \tag{5}$$

where TP is the number of true positives, TN is the number of true negatives, FP is the number of false positives, FN is the number of false negatives, $n$ is the number of compounds selected by the model, $N$ is the total number of entries in the database, and $A$ is the total number of active compounds in the database. In this use, a *positive* compound is one identified to be active by the model, while a *negative* compound is identified to be inactive by the model. The term *true* indicates the result from the model agrees with the experimental result, while *false* indicates a result from the model that disagrees with the experimental result. For example, a true positive is a compound predicted by the model to be active that is experimentally active and a false positive is a compound predicted by the model to be active that is experimentally inactive. For Eqs. (1)–(3), and (5), a value closer to one indicates better performance. For Eq. (4), values greater than one indicate performance better than random selection.

### 2.3. Database searching

Database searching was performed in the 3D compound database, which contains up to 10 conformations per molecule, downloaded from the PubChem FTP site (ftp://ftp.ncbi.nlm.nih.gov/pubchem/Compound_3D/10_conf_per_cmpd/). The compounds were imported into MOE 2012.10 and the 3rd generation model was used to query the database. The number of compounds returned from the database search was reduced by excluding anything with a Log $P$ below 1.7 and above 5.9. These values represent the Log $P$ values of compounds **#25** and **#39,** respectively and were used because they are the highest and lowest Log $P$ values of the most potent activators. The molecular weights of compounds **#25** and **#39** were used to further reduce the number of compounds by excluding those whose molecular weight fall outside the range of 198.2620–455.7030 g/mol. Finally, since the steroid recognition site is located in the transmembrane part of the helix, compounds that would be too polar for membrane insertion were removed. This was accomplished by calculating the number of non-carbon heavy atoms in each molecule. Any compound with more than four non-carbon heavy atoms was removed from the hit list, since all but one known active (**#20**) contain no more than four non-carbon heavy atoms.

Clustering was performed on the remaining compounds by first calculating MACCS structural keys (a binary description of structure) [26] and similarity was determined using a 65% Tanimoto coefficient (a measure of similarity between two compounds) [27] similarity threshold. The clustering overlap threshold was set at 65% or greater; meaning two compounds would require 65% or greater Tanimoto similarity among their structural neighbor lists to be placed in the same cluster. The formal charge on compounds in each cluster was used to further reduce the number of compounds by eliminating compounds with no formal charge, leaving only compounds with −1 or −2 charges to mimic the charge on the most active compounds (LCA and 3-HENA).

### 2.4. Automated patch clamp procedures on recombinant $BK_{Ca}$

#### 2.4.1. Cell culture

Recombinant $BK_{Ca}$ channel-forming cbv1 (AY330293) and accessory β1 (FJ154955) subunits cloned from rat cerebral artery myocytes [28,29] were stably expressed in the human embryonic kidney (HEK) 293 cell line (ATCC). Cells were grown in sterile tissue flasks in Dulbecco's modified eagle medium (DMEM; Cellgro) supplemented with 10% (v/v) heat-inactivated fetal calf serum (FCS; Hyclone) and penicillin:streptomycin (6:100 μg per 1 mL) solution (Cellgro) at 35 °C in 5% $CO_2$. Confluent cell cultures were sub-cultured every 2–3 days. Before electrophysiological experiments, cells were treated with trypsin/EDTA (Invitrogen) for 1 min at 35 °C, in 5% $CO_2$, harvested, and centrifuged at 1000 rpm for 5 min. The pellet was washed once with PBS (Cellgro), and the resulting cell suspension was centrifuged again. The pellet was gently re-suspended in the extracellular solution and used for electrophysiological recording.

#### 2.4.2. Solutions

The extracellular solution was buffered to pH 7.4 with an overall osmotic concentration of 298 mOsm and contained (mM): NaCl 140; KCl 4; $CaCl_2$ 2; $MgCl_2$ 1; D-glucose monohydrate 5; HEPES 10. The seal enhancing solution was buffered to pH 7.4 and contained (mM): NaCl 80; KCl 3; $MgCl_2$ 10; $CaCl_2$ 35; HEPES 10. The internal $Ca^{2+}$-free solution was buffered to pH 7.2 and contained (mM): KCl 50, NaF 10; KF 60; EGTA 5; HEDTA 1.6; HEPES 10; $MgCl_2$ 2.28. For vehicle- or compound-containing solution internal solution was supplemented by a $Ca^{2+}$/EGTA stock (1/0.1 M) to render nominal 10 μM $Ca^{2+}$. The nominal free $Ca^{2+}$ concentration was calculated with MaxChelator Sliders (C. Patton, Stanford University). All solutions were filtered through 0.45 μM Millex filter unit (Millipore) and stored for no more than 1 week at +4 °C.

#### 2.4.3. Compounds

Sobetirome was purchased from APExBIO; PubChem CID 3307939 and 7312086 from MCULE. The remaining compounds were purchased from Cayman Chemical. A 1/9 (v/v) DMSO/EtOH mixture was used as vehicle. The stock solution for each compound

**Table 1**
Distance constraints used in NCI database searching.

| Pharmacophore points | Lithocholic acid distances | NCI search distances |
|---|---|---|
| 1 → 2 | 4.93 Å | 4.60Å → 5.80 Å |
| 1 → 3 | 10.48 Å | 9.00Å → 11.00 Å |
| 2 → 3 | 7.28 Å | 6.50Å → 8.30 Å |

was prepared at 333 mM using the aforementioned mixture. On the days of the experiment, the compound stock solution was diluted in the extracellular recording solution to 45 μM. This concentration represents the $EC_{50}$ for the $BK_{Ca}$ channel activator lithocholic acid [12]. The DMSO/ethanol vehicle (≤0.015/≤0.13% final concentrations) in the extracellular solution was used as control.

*2.4.4. Patch-clamp recording on patchliner (Nanion Technologies)*

On the day of the experiment, a 500-mL aliquot of the cell suspension in the extracellular solution was placed in the cell-hotel. Cells were added to each chip well and attracted to the holes by suction applied by a pressure controller. Once a stable whole-cell configuration was obtained, the experimental protocol was initiated. $K^+$ currents were measured with a patch-voltage-clamp technique in the whole-cell configuration at room temperature using the Quadro EPC-10 amplifier and associated PatchMaster software (HEKA Elektronik). Currents were low-pass filtered using the internal Bessel filter of the EPC-10 and digitized at 50 kHz. Whole-cell ionic currents were evoked from a holding potential of −80 mV by 200 ms long, 10 mV steps ranging from −150 to +150 mV. After whole-cell currents were recorded in control, vehicle-containing solution, the extracellular solution was switched to the compound solution. Cells were incubated with compound for 20 s, and the currents were recorded. Between the compounds, the patchliner pipette was washed with 2% DMSO.

*2.4.5. Data analysis*

Measurement of the whole-cell $BK_{Ca}$ current amplitude at each voltage step was performed using PatchMaster software (HEKA Electronik) 100 ms after the start of the depolarizing step. Macroscopic conductance $G/G_{max}-V$ plots were fitted to a Boltzmann function of the type $G_{(V)} = G_{max}/1 + \exp[(-V + V1/2)/k]$. Boltzmann fitting routines were run in Origin software (OriginLab) that was also used for the final fitting and plotting of the data. As a measure of channel activity we used $V_{half}$, i.e., the voltage needed to reach half-maximal macroscopic conductance. Therefore, a decrease in $V_{half}$ indicates an increase in $BK_{Ca}$ current while an increase in $V_{half}$ reflects a reduction in $BK_{Ca}$ current, independently of changes in ion channel expression. Statistical analysis was conducted by InStat 3.0 (GraphPad) using one-way analysis of variance and Bonferroni's multiple comparison test. $P < 0.05$ was considered statistically significant. Data are expressed as mean ± S.E.M., and ($n$) = number of cells. Each cell was only tested once with control (vehicle) and a single compound.

## 3. Results and discussion

### 3.1. Model selection

For the 1st generation model, three points were established on the LCA molecule. These points were based in part on a previous study [22]; two points underscored the importance of the lateral chain carboxylic acid and the A ring hydroxyl. A carbon in the steroid nucleus was selected as the third point to represent the concavity of LCA due to a cis A–B ring junction and is shown in Fig. 3A. The distances between the points and the ranges used to search the NCI database are shown in Table 1. Since LCA has a Log $P$ of 6.05, a Log $P$ range of 4–8 was also used as additional search criteria to narrow the results. Due to the limitations of the browser-based search features of the NCI database and limited availability of compounds in that database, this method was abandoned in favor of more robust three-dimensional model development using MOE. While the 1st generation model provided a starting point, it was inherently limited to 3D distance descriptions of the pharmacophore and did not involve inactive compounds for model development.

The 2nd generation pharmacophore used LCA and deoxycholic acid as active compounds to develop the model and provided a more robust description of the steroid recognition site in $\beta_1$ by using four features to describe the pharmacophore in three dimensions (Fig. 3B). The set of potential models was analyzed for hydrophobic features that were spaced to convey the "bean" shaped concavity of LCA. Candidate models were also screened using the criteria that the model should contain a hydrogen bond donor feature aligned with the hydroxyl of LCA and a hydrogen bond acceptor feature aligned with the carboxylate of LCA as these two functional groups very likely play a role in the interaction with $\beta_1$ based on previous SAR, modeling and mutagenesis studies reported by our groups [13,16,22,30,31]. The top candidate model was tested for accuracy using a test set of compounds with experimentally known activity on $\beta_1$-containing $BK_{Ca}$ channels that excluded the compounds used to train all models so that all models were evaluated using the same set of compounds.

For the 3rd generation model, the top candidate model was selected from the potential models using the same selection criteria as the 2nd generation model. An additional feature, however, was allowed in the 3rd generation model: a carboxylate ion bioisostere feature that allows other functional groups in place of the carboxylate (Fig. 3C).

The top candidate pharmacophore model in the 4th generation was selected using the previously mentioned criteria for the 2nd generation model, but the placement of hydrophobic features was more heavily scrutinized than previously. This was accomplished by ensuring any candidate models had hydrophobic features in the steroid nucleus of the active molecules and not on methyl groups (Fig. 3D).

For the 6th generation model, the two top models ranked by the model development algorithm were selected to evaluate with the test set. The models differed only in the first feature, where the top model had a hydrogen bond donor projection and the second ranked model had a hydrogen bond acceptor projection. These projections place pharmacophore features on the projected interaction sites for hydrogen bond donor and acceptor atoms in a molecule and could find a partner hydrogen bond acceptor or donator interaction partner common to all activators of the cholane steroid-recognition site. The second model was selected as the 6th generation model after evaluation of performance against the test set compounds (Fig. 3E).

Distances between pharmacophore features in models 2–6 are provided in Table 2 and the radius of each feature is provided in Table 3. Because models are generated using conformational databases of active and inactive compounds, distances between similar features are not necessarily the same. The radii of pharmacophore features were generally left at default values except in the 5th generation model where feature radii were intentionally decreased to increase specificity.

### 3.2. Model performance

The metrics used to evaluate the models are displayed in Table 4. These values are reported because they represent the most commonly reported pharmacophore metrics [25] and because each gives different insight into model performance.

**Table 2**
Distance (Å) between pharmacophore features in generations 2–6.

| Pharmacophore points | 2nd Generation | 3rd Generation | 4th Generation | 5th Generation | 6th Generation |
|---|---|---|---|---|---|
| 1 → 2 | 4.08 | 4.60 | 5.33 | 5.10 | 5.12 |
| 1 → 3 | 9.58 | 9.63 | 11.95 | 11.95 | 7.68 |
| 1 → 4 | 8.99 | 9.00 | 8.57 | 8.57 | 13.00 |
| 1 → 5 | – | 10.18 | – | – | – |
| 2 → 3 | 7.61 | 7.39 | 9.43 | 9.27 | 2.58 |
| 2 → 4 | 5.15 | 4.56 | 4.42 | 4.35 | 8.64 |
| 2 → 5 | – | 7.76 | – | – | – |
| 3 → 4 | 5.68 | 5.97 | 5.42 | 5.42 | 7.16 |
| 3 → 5 | – | 0.63 | – | – | – |
| 4 → 5 | – | 5.96 | – | – | – |

**Table 3**
Radii (Å) of pharmacophore features in generations 2–6.

| Pharmacophore point | 2nd Generation | 3rd Generation | 4th Generation | 5th Generation | 6th Generation |
|---|---|---|---|---|---|
| 1 | 1.4 | 1.4 | 1.6 | 1.0 | 1.0 |
| 2 | 1.4 | 1.4 | 1.4 | 1.3 | 1.4 |
| 3 | 1.4 | 1.4 | 1.6 | 1.3 | 1.4 |
| 4 | 1.4 | 1.4 | 1.4 | 1.3 | 1.4 |
| 5 | – | 1.4 | – | – | – |

The 2nd generation model scored comparably to the 4th and 5th generation models (Table 4) with the standard test set in some calculated metrics, but performed lower in others. Compared to the 4th generation model, this model was 0.07 lower in sensitivity, 0.04 lower in yield of actives, 0.10 lower in enrichment, and 0.03 lower in accuracy. This indicates the inclusion of more recently tested compounds with greater activity in the 4th generation training set led to improvements in model performance.

The 3rd generation model featured a fifth pharmacophore point, which more than doubled the specificity, increased the yield of actives by 0.27, the enrichment by 0.65, and the accuracy by 0.22, but had a sensitivity almost half that of the 2nd generation model with the standard test set. Additionally the 3rd generation model showed the greatest enrichment of any of the models generated. The fifth point was a carboxylate bioisostere intended to improve structural diversity among selected compounds. The low number of true positives and false positives indicate the fifth feature of this model is overly restrictive compared to four feature models. While this fifth feature did improve the model in several metrics, due to the large decrease in sensitivity, the placement and type of feature need to be further refined in future efforts to yield a model that better identifies the active compounds as true positives.

For the 4th generation model, the three most active compounds were used to train the model (**#10, 14, 39**). The drop in specificity, or true negative rate, of 0.54 compared to the 3rd generation model indicates that the 4th generation model cannot correctly eliminate inactive compounds as well as the 3rd generation. This model outperformed the 3rd generation model only in sensitivity by 0.34, so further refinements were sought to improve upon the 4th generation model, without sacrificing sensitivity as was seen in the 3rd generation model.

In an effort to improve specificity of the 4th generation model, the radii of features were reduced and features were moved to the steroid nucleus to yield the 5th generation model. While the specificity did improve to be better than the 2nd generation model by 0.04, the sensitivity, or true positive rate, declined by 0.07 compared to the 4th generation model to become equivalent to the 2nd generation model. Other metrics remained similar between 4th and 5th generation models.

The 6th generation model, which used the newer model development protocol in MOE 2013.08, provided a significant improvement in sensitivity of 0.20 and 0.54 over the previous 4th and 3rd generation models, respectively. The specificity of the model was on par with the 4th generation model, but 0.04 lower than the 5th generation model and 0.54 lower than the 3rd generation model. Accuracy improved to 0.54, which is 0.08 better than the 4th and 5th generation, but 0.09 lower than the 3rd generation model. Enrichment also improved over 4th and 5th generation by 0.16 and 0.18 respectively, but was 0.39 behind the 3rd generation model.

The major difference in sensitivity and specificity for the 3rd and 6th generation models demonstrates the biggest issue with pharmacophore model development for β1 so far. With current models, any increase in sensitivity caused a decrease in specificity. Since the PubChem database contains over 33 million compounds, the more selective nature of the 3rd generation model helps to reduce the number of compounds returned from the search of a database that large, even though some active compounds will not be returned as hits.

**Table 4**
Evaluation metrics for pharmacophore model generations 2–6 using the standard set of test compounds.

| | 2nd Generation | 3rd Generation | 4th Generation | 5th Generation | 6th Generation |
|---|---|---|---|---|---|
| True positives | 9 | 5 | 10 | 9 | 13 |
| False positives | 15 | 3 | 15 | 14 | 15 |
| True negatives | 7 | 19 | 7 | 8 | 7 |
| False negatives | 6 | 10 | 5 | 6 | 2 |
| Sensitivity | 0.60 | 0.33 | 0.67 | 0.60 | 0.87 |
| Specificity | 0.32 | 0.86 | 0.32 | 0.36 | 0.32 |
| Yield of actives | 0.36 | 0.63 | 0.40 | 0.39 | 0.46 |
| Enrichment | 0.89 | 1.54 | 0.99 | 0.97 | 1.15 |
| Accuracy | 0.43 | 0.65 | 0.46 | 0.46 | 0.54 |

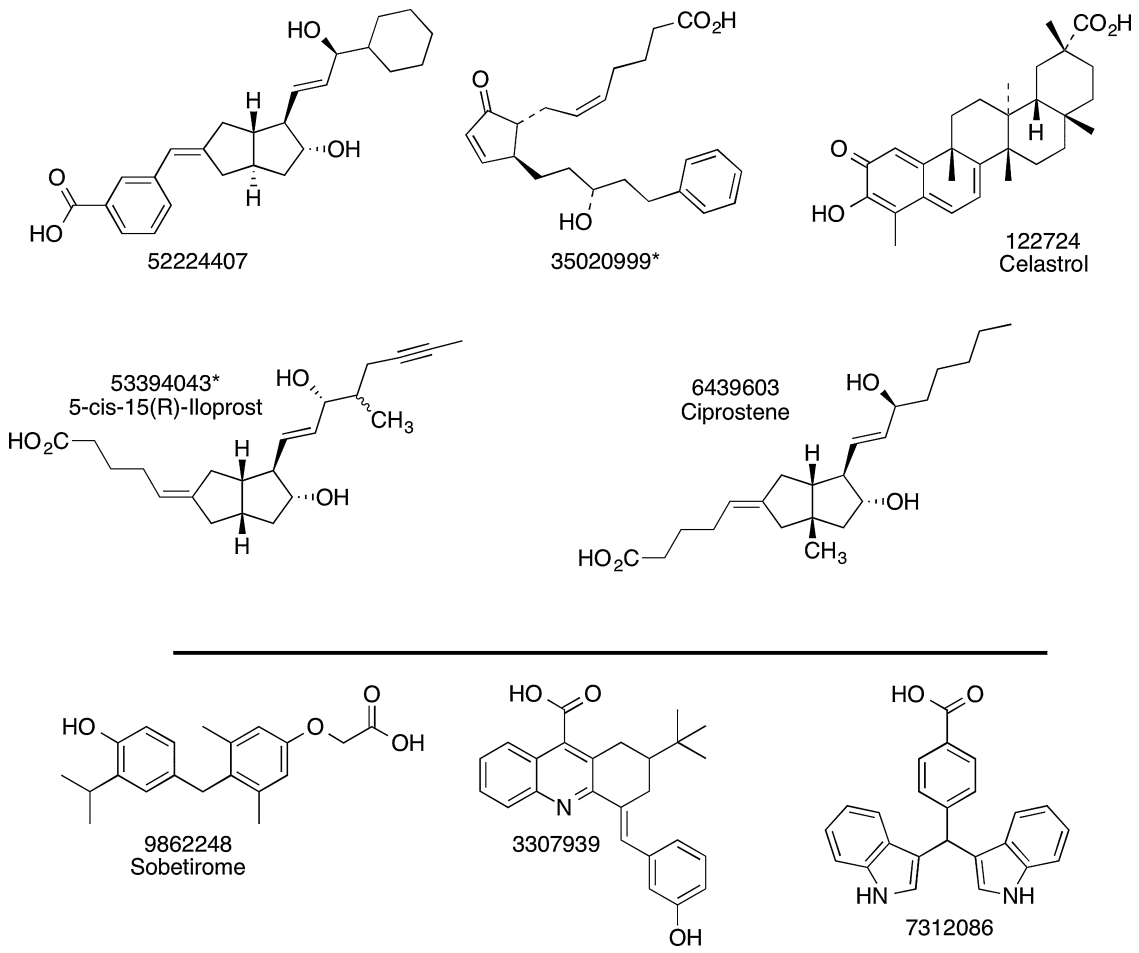


**Fig. 4.** Commercially available compounds selected from PubChem database with compound ID (CID) numbers. Compounds were selected by visual inspection of structural similarity clusters. Compounds above the black line came from the largest cluster of 5429 compounds. Compounds with an asterisk next to the CID were identified by PubChem as similar to a compound originally selected that was no longer commercially available. Common names are given for compounds that have common names.

### 3.3. Virtual screening results

The 1st generation pharmacophore search of the NCI database yielded several compounds, but due to limitations on availability from NCI none of the compounds were available for screening. Also, the limitations of the web browser-based query in the NCI database with distances assigned to atom types led us to pursue a 3D pharmacophore model with feature annotations. However, the distance constraints established for the NCI search were later used to guide development of potential 2nd generation models. Development of 3D models also allows for searching of databases other than NCI. Further database searching in Hit2Lead.com was performed, but similarity to LCA was used instead of the distance constraints used for NCI. This search yielded 3-HENA as discussed in detail by Bukiya et al. [13].

Due to the size of the PubChem database, the 3rd generation model was used for virtual screening due to the high specificity of this pharmacophore generation. Initially, there were 317,771 compounds returned by the model. Due to the laborious nature of visually inspecting over 300,000 compounds, filters were applied to the hit list to further reduce the number of compounds returned by the pharmacophore search. The upper and lower limits of the best known activators were used to filter by molecular weight, Log *P*, and the number of non-carbon heavy atoms. This removed any compounds that were unlikely to be activators based on our current understanding of the pharmacophore by removing compounds that would be too large for the recognition site or too polar for membrane partitioning. Since the inactive compounds have a larger Log *P* range of 0.47–8.0 and a larger molecular weight range of 142.154–516.787 compared to a Log *P* range of 1.7–5.9 and a molecular weight range of 192.262–455.703 for active compounds, using these filters should remove a larger proportion of inactive than active compounds. Additionally, restricting the number of non-carbon heavy atoms reduced the number of compounds that would not insert well into the membrane to access the steroid recognition site. Finally, compounds lacking a formal negative charge were removed from the hit list. This cutoff was selected due to the −1 charge present in the two most potent compounds: LCA and 3-HENA. However, because the synthetic LCA derivative with a nitrile in place of the carboxylic acid functional group is active, this method could potentially remove some active compounds. The total number of compounds was reduced to 7193 after all filters were applied.

Structural similarity clustering of the 3rd generation model search results was accomplished using MACCS structural keys to fingerprint molecules and Tanimoto similarity. A total of 953 clusters were produced at a 65% similarity threshold with the largest cluster containing 2655 compounds.

All clusters were visually inspected to identify promising compounds for screening. The largest cluster included many bile acid derivatives and triterpenoids similar to LCA and 3-HENA, but also contained many compounds with structural diversity compared to current test and training set compounds. Five compounds were selected for screening from this largest cluster, although two

originally selected compounds were substituted with close analogs (stereoisomers) when the originally selected compound proved not to be commercially available (Fig. 4). Three additional compounds from three other clusters were also selected for screening to enhance structural diversity among these candidate $BK_{Ca}$ activators.

### 3.4. Experimental screening results

The selected compounds were screened by automated patch-clamp assay for their ability to activate recombinant channels in HEK293 cells expressing both the $BK_{Ca}$ channel-forming cbv1 and the β1 accessory subunit (Fig. 5). Two of the eight tested compounds, sobetirome and celastrol, reduced $V_{half}$, the voltage needed to reach half-maximal ionic current. These two compounds therefore activate the channel. Given the small size of the screening set, the 25% hit rate needs further verification, but certainly demonstrates the combined ability of the pharmacophore model and the filtering process to select active compounds and to limit the proportion of compounds screened that prove inactive. The fit of the two active compounds and two of the six inactive compounds (ciprostene and PubChem CID 52224407) on the 3rd generation pharmacophore is shown in Fig. 6. All four compounds clearly place appropriate functional groups into the spheres defining the pharmacophore feature locations. Three of the four additionally maintain a concave shape without steric bulk filling the space between the hydrogen bond donor and the carboxylic acid bioisostere. Ciprostene, an inactive compound, fails to exhibit the concave shape that has previously been identified as essential for activity (Fig. 6C) [16,22,31]. The lack of activity observed for PubChem CID 52224407 seems most likely due to the lengthy extension of the molecule outside of the volume defined by the

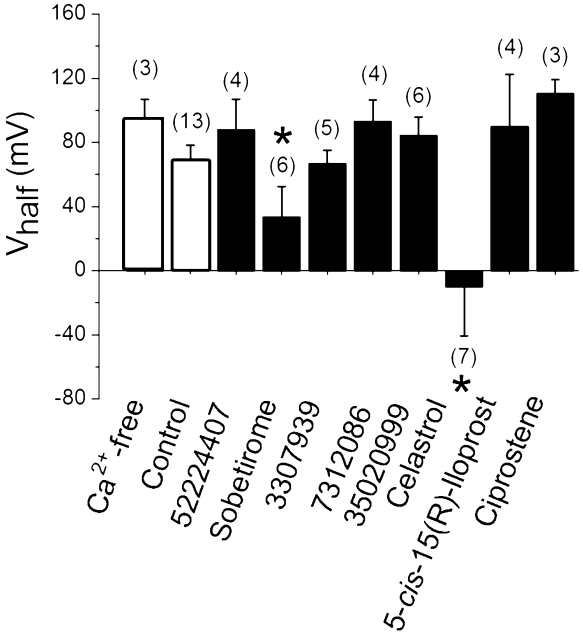


**Fig. 5.** Two $BK_{Ca}$ channel activators were revealed during patch-clamp testing of newly identified compounds. Bar graphs show average $V_{half}$ of $BK_{Ca}$ currents obtained from whole-cell recordings to evaluate the activity of the newly identified compounds. Hollow bars represent data obtained in the absence of compounds. Currents were initially tested in $Ca^{2+}$-free (first hollow bar) versus $Ca^{2+}$-containing (second hollow bar) intracellular solution: the $V_{half}$ shift toward a lower value in presence of $Ca^{2+}$ underscores $Ca^{2+}$-dependent gating, which is a characteristic of $BK_{Ca}$ channels. Black bars correspond to the $BK_{Ca}$ current $V_{half}$ in presence of tested compounds. *$P < 0.05$, significantly different from vehicle-containing control.

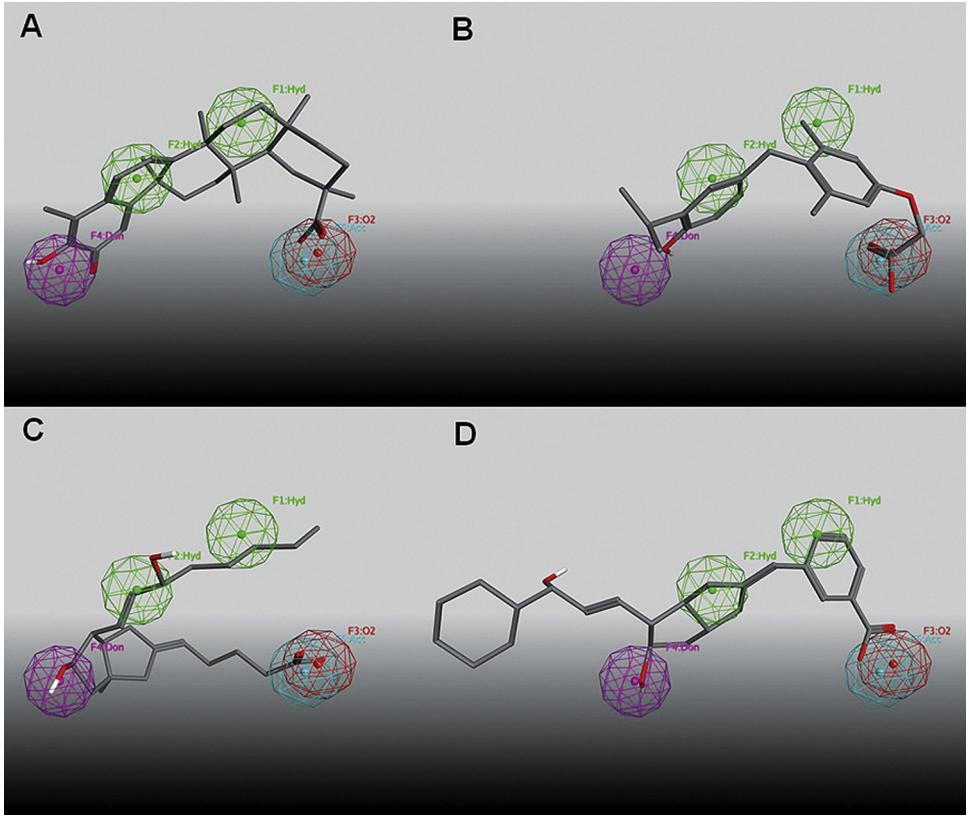


**Fig. 6.** Select commercially available compounds selected from PubChem database superposed on the 3rd generation pharmacophore. Panels A–D exhibit sobetirome, celastrol, ciprostene, and PubChem CID 52224407, respectively.

pharmacophore features (Fig. 6D). Analysis of the fit of both active and inactive compounds on the pharmacophore model will guide the addition of exclusion volumes that can potentially improve sensitivity without a loss in specificity.

## 4. Conclusion

Our pharmacophore model represents a significant step toward the development of a robust tool for the discovery of novel activators of the $\beta_1$ steroid recognition site. While iterative improvements in pharmacophore modeling and new information have advanced the pharmacophore model over time, further improvements are still needed to address the issues with sensitivity and enrichment without the need for additional filtering. The two active compounds identified in this work represent exciting and structurally novel additions to the set of $BK_{Ca}$ channel activators.

## Acknowledgments

Research reported in this publication was supported in part by the National Institutes of Health under Award Numbers R01-HL103631 (AMD) and R37-AA11560 (AMD). Ms. Camisha Terrell (Christian Brothers University, Department of Chemistry) conducted research at UTHSC Department of Pharmacology under the UTHSC-Christian Brothers University undergraduate summer rotation program. The content is solely the responsibility of the authors and does not necessarily represent the official views of the National Institutes of Health. Provision of MOE by the Chemical Computing Group (ALP) is also appreciated. Authors deeply thank Nanion Technologies team for help in developing protocols for automated patch-clamp $BK_{Ca}$ current recording.

## Appendix A. Supplementary data

Supplementary data associated with this article can be found, in the online version, at http://dx.doi.org/10.1016/j.jmgm.2014.10.008.

## References

[1] R. Lu, A. Alioua, Y. Kumar, M. Eghbali, E. Stefani, L. Toro, MaxiK channel partners: physiological impact, J. Physiol. 570 (2006) 65–72.
[2] B. Eichhorn, D. Dobrev, Vascular large conductance calcium-activated potassium channels: functional role and therapeutic potential, Naunyn-Schmiedeberg's Arch. Pharmacol. 376 (2007) 145–155.
[3] H.G. Knaus, A. Eberhart, G.J. Kaczorowski, M.L. Garcia, Covalent attachment of charybdotoxin to the beta-subunit of the high conductance Ca(2+)-activated K+ channel. Identification of the site of incorporation and implications for channel topology, J. Biol. Chem. 269 (1994) 23336–23341.
[4] P. Meera, M. Wallner, M. Song, L. Toro, Large conductance voltage- and calcium-dependent K+ channel, a distinct member of voltage-dependent ion channels with seven N-terminal transmembrane segments (S0–S6), an extracellular N terminus, and an intracellular (S9–S10) C terminus, Proc. Natl. Acad. Sci. U. S. A. 94 (1997) 14066–14071.
[5] E. Stefani, M. Ottolia, F. Noceti, R. Olcese, M. Wallner, R. Latorre, et al., Voltage-controlled gating in a large conductance Ca2+-sensitive K+channel (hslo), Proc. Natl. Acad. Sci. U. S. A. 94 (1997) 5427–5431.
[6] J.H. Jaggar, V.A. Porter, W.J. Lederer, M.T. Nelson, Calcium sparks in smooth muscle, Am. J. Physiol. Cell Physiol. 278 (2000) C235–C256.
[7] R. Brenner, G.J. Perez, A.D. Bonev, D.M. Eckman, J.C. Kosek, S.W. Wiler, et al., Vasoregulation by the beta1 subunit of the calcium-activated potassium channel, Nature 407 (2000) 870–876.
[8] T. Chang, L. Wu, R. Wang, Altered expression of BK channel beta1 subunit in vascular tissues from spontaneously hypertensive rats, Am. J. Hypertens. 19 (2006) 678–685.
[9] G.V. Petkov, A.D. Bonev, T.J. Heppner, R. Brenner, R.W. Aldrich, M.T. Nelson, Beta1-subunit of the Ca2+-activated K+ channel regulates contractile activity of mouse urinary bladder smooth muscle, J. Physiol. 537 (2001) 443–452.
[10] C.G. Ponte, O.B. McManus, W.A. Schmalhofer, D.M. Shen, G. Dai, A. Stevenson, et al., Selective, direct activation of high-conductance, calcium-activated potassium channels causes smooth muscle relaxation, Mol. Pharmacol. 81 (2012) 567–577.
[11] A. Nardi, S.P. Olesen, BK channel modulators: a comprehensive overview, Curr. Med. Chem. 15 (2008) 1126–1146.
[12] A.N. Bukiya, J.X. Liu, L. Toro, A.M. Dopico, Beta(1) (KCNMB1) subunits mediate lithocholate activation of large-conductance Ca2+-activated K+ channels and dilation in small, resistance-size arteries, Mol. Pharmacol. 72 (2007) 359–369.
[13] A.N. Bukiya, J.E. McMillan, A.L. Fedinec, S.A. Patil, D.D. Miller, C.W. Leffler, et al., Cerebrovascular dilation via selective targeting of the cholane steroid-recognition site in the BK channel beta1-subunit by a novel nonsteroidal agent, Mol. Pharmacol. 83 (2013) 1030–1044.
[14] A.M. Dopico, J.V. Walsh Jr., J.J. Singer, Natural bile acids and synthetic analogues modulate large conductance Ca2+-activated K+ (BKCa) channel activity in smooth muscle cells, J. Gen. Physiol. 119 (2002) 251–273.
[15] A.N. Bukiya, T. Vaithianathan, L. Toro, A.M. Dopico, Channel beta2–4 subunits fail to substitute for beta1 in sensitizing BK channels to lithocholate, Biochem. Biophys. Res. Commun. 390 (2009) 995–1000.
[16] A.N. Bukiya, A.K. Singh, A.L. Parrill, A.M. Dopico, The steroid interaction site in transmembrane domain 2 of the large conductance, voltage- and calcium-gated potassium (BK) channel accessory beta1 subunit, Proc. Natl. Acad. Sci. U. S. A. 108 (2011) 20207–20212.
[17] Y. Wu, Y. Yang, S. Ye, Y. Jiang, Structure of the gating ring from the human large-conductance Ca(2+)-gated K(+) channel, Nature 466 (2010) 393–397.
[18] E.E. Bolton, Y. Wang, P.A. Thiessen, S.H. Bryant, PubChem: integrated platform of small molecules and biological activities, Ann. Reports Comput. Chem. 4 (2008) 217–241.
[19] Molecular Operating Environment (MOE), Chemical Computing Group Inc., Montreal, QC, Canada, 2013.
[20] T.A. Halgren, Merck molecular force field. 1. Basis, form, scope, parameterization, and performance of MMFF94, J. Comput. Chem. 17 (1996) 490–519.
[21] A.N. Bukiya, S.A. Patil, W. Li, D.D. Miller, A.M. Dopico, Calcium- and voltage-gated potassium (BK) channel activators in the 5beta-cholanic acid-3alpha-ol analogue series with modifications in the lateral chain, ChemMedChem 7 (2012) 1784–1792.
[22] A.N. Bukiya, J. McMillan, A.L. Parrill, A.M. Dopico, Structural determinants of monohydroxylated bile acids to activate beta 1 subunit-containing BK channels, J. Lipid Res. 49 (2008) 2441–2451.
[23] S. Patil, A.N. Bukiya, W. Li, A.M. Dopico, D. Miller, Design and synthesis of hydroxy-alkynoic acids and their methyl esters as novel activators of BK channels, Bioorg. Med. Chem. Lett. 18 (2008) 3427–3430.
[24] P. Labute, LowModeMD – implicit low-mode velocity filtering applied to conformational search of macrocycles and protein loops, J. Chem. Inf. Model. 50 (2010) 792–800.
[25] N. Triballeau, H.O. Bertrand, F. Acher, Pharmacophores and Pharmacophore Searches, Wiley-VCH, Weinheim, Germany, 2006.
[26] Machine Learning: Paradigms and Methods, MIT Press, Cambridge, MA, 1990.
[27] D.J. Rogers, T.T. Tanimoto, A computer program for classifying plants, Science 132 (1960) 1115–1118.
[28] A.N. Bukiya, J.X. Liu, A.M. Dopico, The BK channel accessory beta(1) subunit determines alcohol-induced cerebrovascular constriction, FEBS Lett. 583 (2009) 2779–2784.
[29] J.H. Jaggar, A. Li, H. Parfenova, J. Liu, E.S. Umstot, A.M. Dopico, et al., Heme is a carbon monoxide receptor for large-conductance Ca2+-activated K+ channels, Circ. Res. 97 (2005) 805–812.
[30] A.N. Bukiya, T. Vaithianathan, L. Toro, A.M. Dopico, The second transmembrane domain of the large conductance, voltage- and calcium-gated potassium channel beta(1) subunit is a lithocholate sensor, FEBS Lett. 582 (2008) 673–678.
[31] A.N. Bukiya, J. McMillan, A.L. Fedinec, C.W. Leffler, A.L. Parrill, A.M. Dopico, Sodium 3-hydroxyolean-12-en-30-Oate is a novel and selective activator of beta 1 subunit-containing BK channels and thus cerebral artery dilator, Biophys. J. 102 (2012) 133a–134a.